International Journal of Multiphase Flow 35 (2009) 363–375

Contents lists available at ScienceDirect

International Journal of Multiphase Flow

journal homepage: www.elsevier.com/locate/ijmulflow

Unsteady dynamics of Taylor bubble rising in vertical oscillating tubes

S. Madani, O. Caballina *, M. Souhar

LEMTA, Nancy-University, CNRS UMR 7563, 2 avenue de la Forêt de Haye, BP. 160, 54504 Vandoeuvre-les-Nancy Cedex, France

ARTICLE INFO

Article history:
Received 8 May 2008
Received in revised form 5 January 2009
Accepted 13 January 2009
Available online 23 January 2009

Keywords:
Taylor bubble
Oscillating frame
High Reynolds number
Surface tension effect

ABSTRACT

The present work deals with the motion of a Taylor bubble rising through vertical oscillating pipes. The aim is to perform a more detailed and quantitative study of this unsteady flow, still seldom addressed in the literature. The investigation is restricted to high Reynolds numbers to understand inertia effects. Experimental results are provided for two different configurations: (1) pipes with two different inner diameters (9.8 mm and 20 mm) filled with water, (2) the thinner pipe ($D = 9.8$ mm) filled with four low viscous fluids. So the Bond number *Bo* based on the steady rise velocity varies from 13 to 57, where the effects of surface tension can be considered. The bubble trajectory is tracked by using a high-speed video camera. The average terminal and fluctuating velocity, as well as the phase shift with the oscillating plate are obtained by using image processing. The main results show that for weak acceleration, the mean velocity decreases with the relative acceleration as the fluctuating velocity increases in proportion to this acceleration. Beyond a critical relative acceleration, the average velocity increases and the fluctuating velocity increase seems to slow down. Additionally, comparisons are made with experimental results of Brannock and Kubie [Brannock, D., Kubie, J., 1996. Velocity of long bubbles in oscillating vertical pipes. Int. J. Multiphase Flow 22, 1031–1034] and numerical results of Clanet et al. [Clanet, C., Heraud, P., Searby, G., 2004. On the motion of bubbles in vertical tubes of arbitrary cross-sections: some complements to the Dumitrescu Taylor problem. J. Fluid Mech. 19, 359–376].

1. Introduction

Among two-phase flow regimes in a vertical pipe, slug flow appears in a very wide range of flowing conditions. This kind of flow is characterized by large elongated bubbles, also called Taylor bubbles or gas slugs, which nearly occupy the entire cross section of the pipe. A thin film of liquid flows between the gas interface and the pipe wall.

Slug flows occur in several industrial applications. It is useful in desalination industry, in heat exchangers, boilers and heat pipes in order to improve the efficiency by increasing the mass and heat transfer. Slug flow is also widely encountered in the oil extraction industry where it is very undesirable. It causes serious mechanical process and corrosion problems in oil field facilities. Thus it is essential to predict slugging characteristics so as to be able to reach a safe, economic and efficient design in applications such as these. Thus many researchers have been interested in Taylor bubble flow and various investigations have been carried out on this subject. In order to understand the hydrodynamics of such a complex flow, the first step has been to study a single gas slug evolving in a vertical pipe.

The rise velocity of Taylor bubbles depends on the pipe diameter and its inclination angle, the physical properties of gas and liquid phases (density, viscosity and surface tension), and the flow rates of the two phases. White and Beardmore (1962) established by using dimensional analysis, the main dimensionless numbers which govern the motion of Taylor bubbles in pipes: Bond ($Bo = g(\rho_L - \rho_G)D^2/\sigma$), Froude ($Fr = U_b/\sqrt{gD}$) and Morton ($Mo = g\mu_L^4/\rho_L\sigma^3$) numbers, where D is the pipe diameter, U_b is the Taylor bubble mean velocity, ρ_L and ρ_G are the liquid and gas densities, μ_L is the viscosity of the liquid, σ stands for the surface tension and g is the gravity. Other dimensionless numbers could be used, e.g., Collins et al. (1978) used Froude number as a unique function of Morton number and a dimensionless inverse viscosity number, N_f, given by $N_f = \rho_L g^{\frac{1}{2}} D^{\frac{3}{2}}/\mu_L$ ($\sim Re$). It is known that in cylindrical tubes of diameter D, for a Taylor bubble motion in a liquid of kinematic viscosity ν, high Reynolds number bubbles ($Re \equiv U_b D/\nu \gg 1$) are characterized by:

$$U_b = Fr\sqrt{gD} \tag{1}$$

The first studies on the bubble rise velocity in circular cross section pipes and in stagnant fluids, were carried out by Dumitrescu (1943), Davies and Taylor (1950). These studies were limited to the case of bubbles moving in low viscous liquids and where the surface tension effects were considered to be negligible. According to the literature, these conditions are satisfied when $N_f > 300$ (negligible viscosity regime) and $Bo > 100$ (negligible surface tension). In this case, the theoretical solution for a bubble rising in a stagnant column, is given by Eq. (1) where the Froude number is constant. The estimated Froude number by Dumitrescu (1943), Davies and

* Corresponding author. Tel.: +33 383 595 669; fax: +33 383 595 551.
E-mail address: ophelie.caballina@ensem.inpl-nancy.fr (O. Caballina).

0301-9322/$ - see front matter © 2009 Elsevier Ltd. All rights reserved.
doi:10.1016/j.ijmultiphaseflow.2009.01.002

Taylor (1950) is 0.351 and 0.328, respectively. Comparison with experimental results of White and Beardmore (1962), Nicklin et al. (1962), Zukoski (1966) indicates that Dumitrescu's estimate of the Froude number $Fr = U_b/\sqrt{gD}$ is the most accurate one and agrees well with experiment. Dumitrescu also studied the effect of surface tension by investigating the influence of the interface curvature. He observed the bubble propagation in tubes whose diameter is comparable with the capillary length $l_c = \sqrt{2\sigma/\rho g}$. His experimental results for air bubbles in water showed that Eq. (1) is valid only within the limit $D/l_c > 4\sqrt{2}$ or $Bo > 64$. Below this limit, Fr is no longer constant but decreases as the Bond number, $(Bo = 2(D/l_c)^2)$ does. The effects of surface tension were also studied by other authors. Tung and Parlange (1976), Bendiksen (1985) investigated theoretically the influence of surface tension on bubble motion. Both found that surface tension monotonically reduces the rise velocity and this was in agreement with their experiments as well as with the experiments of Zukoski (1966). The simplified result of Bendiksen given by Fabre and Line (1992) can be written as:

$$Fr = 0.344\frac{1-0.96\exp(-0.0165Bo)}{(1-0.52\exp(-0.0165Bo))^{3/2}}\sqrt{1+\frac{20}{Bo}\left(1-\frac{6.8}{Bo}\right)} \quad (2)$$

Thus in a quiescent fluid with moderated viscosities, the velocity U_b can be calculated from a relationship $Fr = f(Bo)$. For Taylor bubbles in co-current flow, the rise velocity can be predicted from Nicklin's equation (Nicklin et al., 1962) $U_b = U_{b_0} + C_0 U_m$, where U_m is the mean velocity of liquid flow in the pipe and U_{b_0} is the Taylor bubble velocity in stagnant conditions. Coefficient C_0 takes value of around 1.2 when the liquid flow is turbulent and around 2.0 when it is laminar.

van Hout et al. (2002) were one of the first ones to perform PIV measurements in slug flow for air–water systems, for stagnant water in the pipe. They determined separately the flow pattern around a single gas slug and the bubble shape. In recent works, this subject was studied for the case of Taylor bubble motion in stagnant newtonian and non newtonian liquids (Sousa et al., 2005, Nogueira et al., 2006) and the bubble shape was obtained more precisely by using the simultaneous particle image velocimetry technique (PIV) and pulsed shadow technique (PST).

As reviewed above, several articles have been published on the Taylor bubble motion in vertical tubes in the case of steady flow. However, in almost all the industrial processes, the flow is unsteady, for example when the pipe undergoes vibrations. In this condition the steady models presented in previous works could not be validated. Unfortunately this subject has remained largely unaddressed.

Brannock and Kubie (1996) were the first to perform an experimental investigation on the motion of Taylor bubbles in 2 m long vertically oscillating vertical pipes with internal diameters of 22 and 44 mm. They were subjected to a perfect sinusoidal vertical motion with the oscillation amplitudes b of 50, 100 and 200 mm and acceleration $b\omega^2$ of 0 (stationary vertical pipe), 1, 5, 10 and 15 ms^{-2} with ω the angular frequency. In all these cases, rise velocity decrease with the relative acceleration $a = b\omega^2/g$ was observed. They indicated a good agreement between the experimental data and their semi-empirical approach. In order to predict this decrease, Brannock and Kubie (1996) assumed that the instantaneous bubble velocity, $U_b(t)$, can be deduced from Eq. (1) by replacing g by g_E where g_E is a "pseudo" effective acceleration. They proposed: $g_E = max[(g + b\omega^2 sin\omega t), 0]$. This choice is not very clear and is not based on any scientific argument. Its only interest is to have a positive quantity under the root of Eq. (1) when the relative acceleration a becomes greater than 1. Then the average bubble velocity was calculated by: $\bar{U}_b = (1/T)\int_0^T U_b(t)dt$, where T is the periodic time. Comparing with their experimental results, they found that the "theoretical" results underpredict the reduction in $\bar{U}_b/U_{b_0}$. Thus by considering the bubble nose distortions which become more important at high relative accelerations, they introduced a critical relative acceleration a_c, at which the bubble is completely broken up, in the rise velocity expression and they proposed:

$$\bar{U}_b/U_{b_0} = \left(1-\frac{a}{a_c}\right)^{\frac{n}{2}}\frac{1}{T}\int_0^T (max[(1+a\sin\omega t), 0])^{1/2}dt \quad (3)$$

where U_{b_0} is the velocity of the Taylor bubble at $\omega = 0$. The critical relative acceleration, a_c, and the exponent n was found experimentally to be equal to 1.7 and 0.05, respectively. Kubie (2000) also studied experimentally the velocity of long bubbles in horizontally oscillating vertical tubes, but this configuration is different of our investigation. In this last case, Kubie (2000) found that the velocity ratio increases with the relative acceleration, a.

Clanet et al. (2004) developed an analytical model in order to analyze the propagation of Taylor bubble in an oscillating vertical tubes. It should be noted that in their case the surface tension effects are considered to be negligible and the bubble nose is assumed to be undeformable. By projection of the Euler equation onto the interface and by assuming a potential motion along the bubble, they obtained the following differential equation:

$$\frac{dU_b}{dt} + k_0 U_b^2 - g(1 - a\sin\omega t) = 0 \quad (4)$$

where $k_0 = 7.66/D$ leading to a $Fr = 0.361$ for steady state regimes. Clanet et al. decomposed the velocity $U_b(t)$ into a mean and fluctuating part: $U_b(t) = \bar{U}_b + U_f(t)$ and used a numerical method in order to determine $\bar{U}_b$. They found that the mean velocity reaches zero for a critical reduced acceleration, a_c of about 1.7 which is in good agreement with the experimental observations of Brannock and Kubie (1996).

Madani et al. (2007) carried out an experimental investigation on the motion of a Taylor bubble moving in water under gravity and vertical oscillating motion generated by a vibrating plate. Their experiments were carried out for different frequencies where the oscillation magnitude b was equal to 5 mm and 20 mm. A very small influence of the oscillation amplitude on the bubble velocity was observed for weak relative accelerations. The evolution of the bubble length for different frequencies were investigated and the small linear evolution of bubble length with the oscillating plate was observed. The effects of quasi-steadiness were also studied by determining Froude and Bond numbers and were found to be more important for high frequencies.

In the present study, this work is extended for different pipe diameters and by using other fluid–gas combinations. As referred above, only two other researchers focused on the unsteady flow of Taylor bubbles and they were only interested in the mean rise velocity of long bubbles. So it appeared legitimate to us to start an experimental study on this topic in order to understand the complex nature of slug flows in quasi-steady conditions. In this work, we carry out an experimental investigation on the motion of a Taylor bubble moving in a non viscous (low viscosity) quiescent liquid under gravity and vertical oscillating motion generated by a vibrating plate. The bubble motion is obtained by using high-speed video tracking and subsequent image processing methods. The average rise velocity, the fluctuating velocity, the phase shift with the oscillating plate are measured. From these results, the effects of quasi-steadiness are studied by defining and determining two unsteady dimensionless numbers: Froude and Bond numbers.

2. Experimental set-up, measurement techniques and data processing

2.1. Experimental set-up

The experimental facility consists of a mechanical system containing a vertically oscillating plate and a closed column filled with a low viscous fluid and a small quantity of gas to generate the Taylor bubble (Fig. 1).

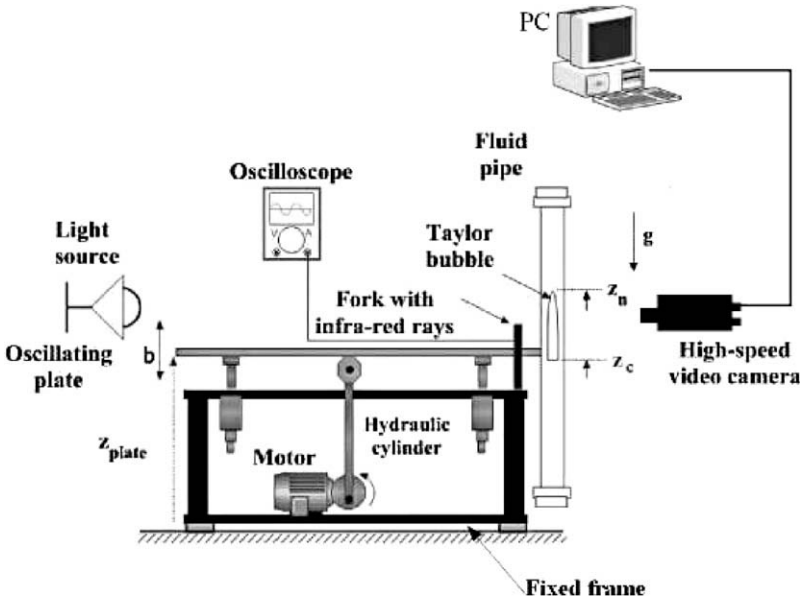

Fig. 1. Sketch of the experimental set-up.

This oscillating system is discussed in more details in Abbad and Souhar (2004).

The mechanical system includes a fixed heavy steel frame and a light plate, being able to carry out a vertical sinusoidal motion. This oscillating motion is obtained by using four hydraulic cylinders fixed at the frame and an electric motor to which a steel disc is fixed. A connecting rod fixed on one side at the disc, and on the other side at the plate, transforms the rotational movement of the motor into the vertical oscillatory motion of the plate. In this study the oscillation amplitude b is equal to 5 mm and the rod length L is 500 mm. In this case the small ratio b/L allows a quasi-perfect sinusoidal motion (Abbad and Souhar, 2004) modeled by:

$$z_{plate} \simeq b\sin(\omega t) \tag{5}$$

The oscillation frequencies can go up to 10 Hz. They are measured by means of an infra-red ray emitting fork fixed at the heavy frame and of a screw fixed on one lateral edge of the oscillating plate. By starting the system, the cut-off frequency of the rays by this screw gives us the oscillation frequency of the plate, which can be read by using an oscilloscope.

The two test sections used are vertical cylindrical glass tubes of 1200 mm and 1000 mm in length with respective internal diameters, D, of 9.8 mm and 20 mm. On both ends of each tube, tight stoppers are placed to allow to fill and empty it. On the tube a metal column is fixed with collars. This column is fixed to the oscillating plate by means of a metal stem fixed at the plate and of a housing bearing fixed at the metal column. The fixing system allows the pipe to rotate around the stem axis (Fig. 2). The Taylor bubble is obtained by two steps. First, a small volume of air is left when filling the tube with the testing fluid. Then the tube is turned around the stem axis and is blocked against a stop after a rotation of 180°. Here, the air volume at the bottom of the pipe with the density lower than water density rises in the form of a Taylor bubble under gravity along the tube. The bubble length, l, is determined by the air volume left in the pipe. The ratio l/D for the two pipe diameters, 9.8 and 20 mm, is about 5 and 3.6, respectively.

2.2. Measurement technique and image processing

The Taylor bubble motion is filmed by means of a high-speed video camera system FASTCAM-ultima APX RS (Photron company) provided with a CMOS sensor of 1024 × 1024 pixels. Images can be recorded at a frequency up to 3000 Hz in full frame, and up to 250,000 at a resolution of 128 × 16. The camera is connected to a PC via an IEEE1394 digital interface and can be controlled using Photron's PFV software. It should be noted that this camera allows for a higher precision than the CCD camera (sensor with 640 × 240 pixels) used previously (Madani et al., 2007).

The camera is fixed on an adjustable support which allows positioning of the camera vertically so as to fit to a field of view where the bubble has reached its average terminal velocity. The use of a LED area backlighting provides a homogeneously diffuse light for high-contrast images. Fig. 3 shows a front view of the experimental set-up. We can see for the example given on this figure that the resolution of the camera is about 0.24 mm pixel^{-1} in z-direction. The images are recorded at 250 images/s with the resolution of 512 × 1024 pixels.

The recorded sequences of the bubble motion are then processed by using the Matlab image processing toolbox. Image analysis consists in determining the bubble nose position as well as the plate position in time. We give an example in Fig. 4 showing the succesive steps of image processing namely: (a) reading of the raw image (Fig. 4a), (b) definition of a region of interest ROI (Fig. 4b), (c) binarization of the ROI by thresholding (Fig. 4c). As we can see when zooming in on the binary images, the bubble nose thickness in almost all the cases is about 4 pixels. The bubble nose detection consists in finding two black pixels corresponding to the maximum z-coordinate on the external and on the internal bubble nose. The nose z-coordinate z_n will be the average of these two values. The same procedure is undertaken to extract the motion of the oscillating plate z_{plate} by locating graduations of a ruler fixed on the support of the pipe (Fig. 4c and d). It should be pointed out that the camera and so the measurements of z_n are done in the fixed reference frame.

2.3. Data processing

In the field of view, the nose position $z_n(t)$, the relative position $z_r(t) = z_n(t) - z_{plate}(t)$, and the relative velocity of the Taylor bubble $U_r(t)$ in the first approximation can be formulated as:

$$z_n(t) = z_{n_0} + z_{n_1}\sin(\omega t + \phi_n) + \bar{U}_b t \tag{6}$$

$$z_r(t) = z_{r_0} + z_f\sin(\omega t + \phi) + \bar{U}_b t \tag{7}$$

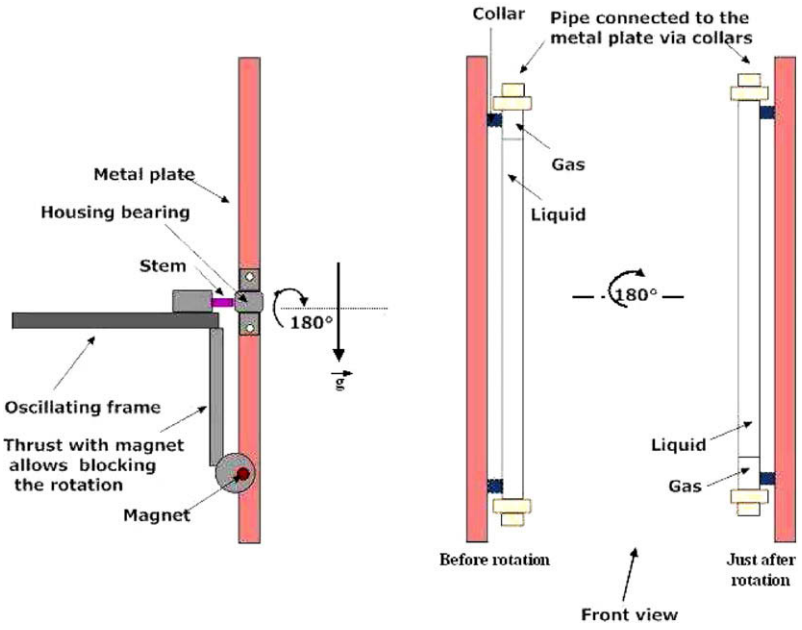

Fig. 2. Rotating system, pipe and metal plate before and after rotation.

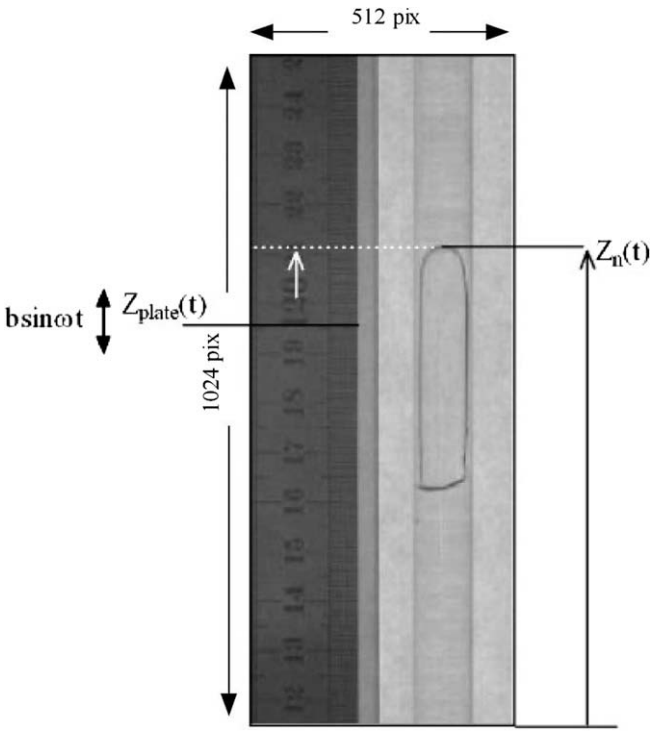

Fig. 3. Photograph of a Taylor bubble rising through 9.8 mm inner-diameter pipe filled with water at $f = 5$ Hz.

and by differentiating the Eq. (7):

$$U_r(t) = U_f \cos(\omega t + \phi) + \bar{U}_b \tag{8}$$

where $\bar{U}_b$ is the mean velocity of the bubble and z_f, U_f and ϕ are, respectively, the displacement magnitude, the fluctuating velocity and the phase shift with the oscillating plate. These different parameters are determined by an optimization technique using the nonlinear least squares method (see Coleman and Li (1996)).

The accuracy of the model function is checked by examining the residue ($Rz = z_{opt} - z_{mes}$), difference between the measured trajectories z_{mes} and the modeled trajectories z_{opt}, which should be a random variable having a null average. Then, the probability function of the residue is compared with the gaussian probability law. Moreover the frequency spectrum of the modeled and measured trajectories are obtained by using a Fourier transform. It is confirmed that the difference between the modeled value and the experimental value is very weak. No variation of amplitude, and no phase shift is generated by the residue.

Phase shifts measurements are very sensitive and are carried out by using an optimization method and also manually. The manual method consists in measuring the delay (τ_s) between the periodic trajectories of the plate and the Taylor bubble. The phase shift is then obtained by the relation $\phi = 2\pi f \tau_s$ with a maximum absolute error of about ±7°.

2.4. Experimental conditions

In our study, two pipes with internal diameters, D, of 9.8 and 20 mm are used. The experiments are carried out for 10 frequencies ranging from 1 Hz to 8.8 Hz, and for the oscillation magnitude b equal to 5 mm. For each frequency, the experiment is repeated at least three times in order to verify the reproducibility and the dispersion of the results is found to be less than ±5%. In the present study, the tests are carried out at temperatures between 18 °C and 22 °C. The physical properties of the four tested liquids are given at 20 °C in Table 1.

3. Results and discussion

As an example, Fig. 5a presents the position of the plate recorded at 250 images/s and for an oscillation frequency of 5 Hz. It is clear that the optimization provides a correct description of the plate trajectory and the maximum frequency deviation is less than 0.2%. The residue $z_{pl_{opt}} - z_{pl_{mes}}$ is very weak, its average is almost zero and follows a gaussian probability law (Fig. 5b). The standard deviation of the residue in this case is $\sigma \simeq 0.15$ mm which is less than one pixel. That is also confirmed in Fig. 5c where the frequency spectrum is illustrated. Only a single significant peak frequency is observed and hence the motion of the plate can be considered as quasi-sinusoidal.

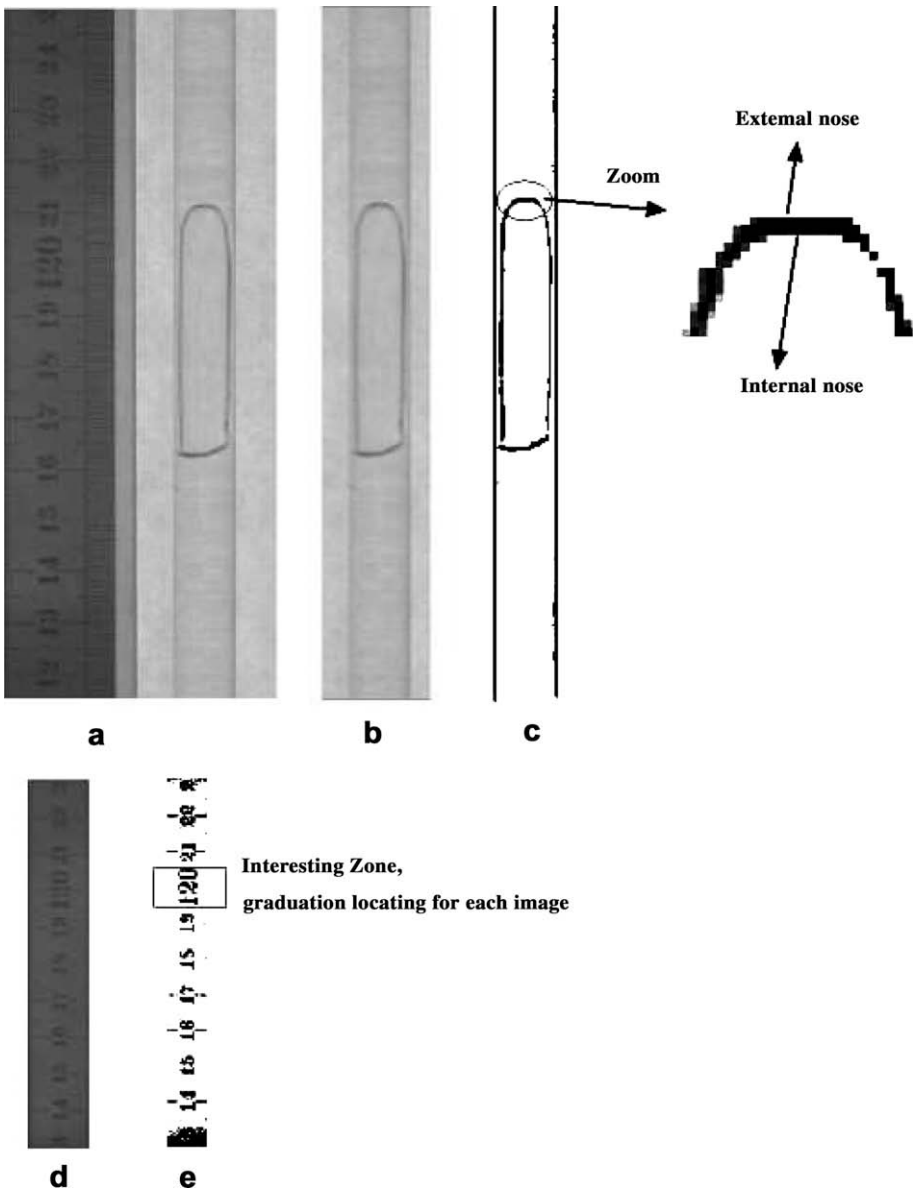

Fig. 4. Steps of image processing: (a) reading the raw image, (b) definition of ROI (test column), (c) binarization, (d) ruler, and (e) binarization ($f = 5$ Hz).

Table 1
Experimental conditions and physical properties of the fluids used at 20 °C.

Fluid	ρ_L (kg m^{-3})	μ_L (mPa s)	σ (mN m^{-1})	D (mm)	$\frac{L_c}{D}$
Water	998	1.05	72	9.8	0.39
Aniline	1020	3.77	43	9.8	0.3
Ethanol	789	1.078	22	9.8	0.23
Carbon tetrachloride	1590	0.901	27	9.8	0.19
Water	998	1.05	72	20	0.19

For the same frequency, the trajectory of the bubble in water is shown in Fig. 6a. The mean rise velocity $\bar{U}_b$ as well as the fluctuating velocity U_f can be deduced from derivatives of the optimized curves. In Fig. 6b, the average motion is subtracted and the bubble oscillation around the zero mean position is plotted. Here again an excellent optimization is observed which can be justified by the residue which has a null average and follows a quasi-gaussian probability law ($\sigma \simeq 0.17$ mm) as shown in Fig. 7a. This can be confirmed from the frequency spectrum (Fig. 7b). The same procedures are carried out for other frequencies and in all cases our approximation model describes correctly the plate and the Taylor bubble trajectory.

3.1. Physical mechanism of the Taylor bubble propagation

In order to understand the physical behavior of the bubble nose in its sinusoidal motion, the temporal evolution of the oscillating plate and the bubble position, namely $z_{plate}(t)$ and $z_{bubble}(t)$, as well as the relative velocity $U_r(t)$ and the effective acceleration $g_E(t)$ are plotted in Fig. 8.

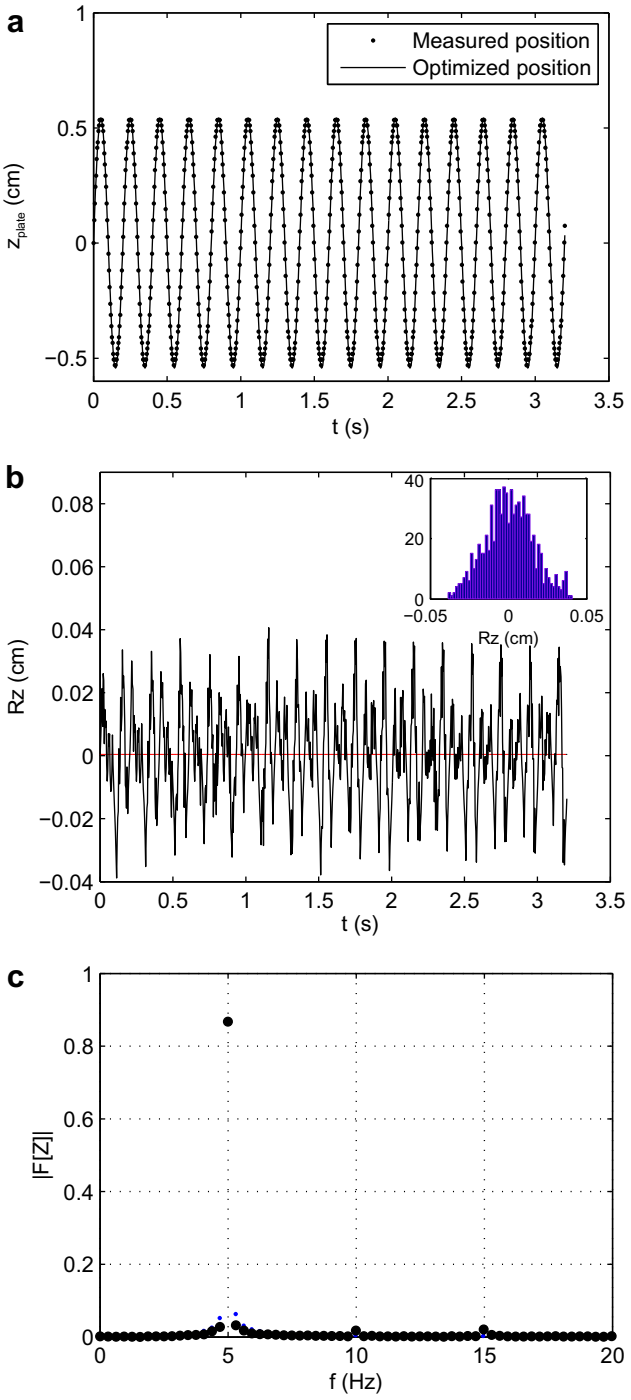

Fig. 5. (a) Measured and optimized positions of the plate, (b) residue between the measured and optimized positions of the plate with histogram of the residue shown in the up-right corner, and (c) spectrum, $f = 5$ Hz and $b = 5$ mm.

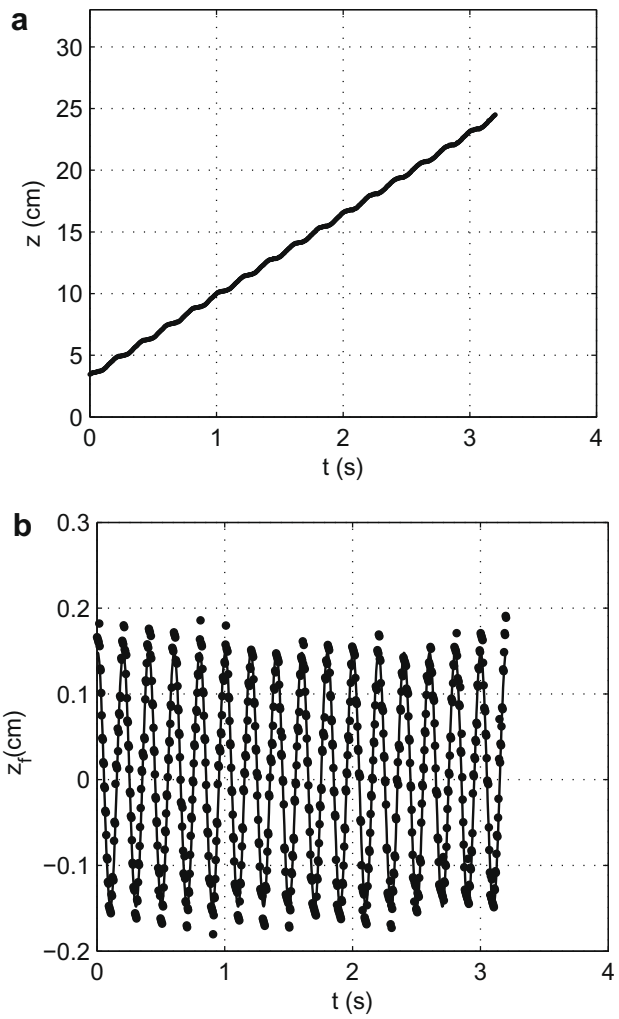

Fig. 6. (a) Measured and optimized positions of the bubble, (b) bubble oscillations around the zero-mean position: •, measured position; –, optimized position, $f = 5$ Hz and $b = 5$ mm.

The analysis of these figures shows that when the plate goes through the position $z_{plate} = 0$, where $g(t) = g$ (point B in Fig. 8a), the relative velocity of the Taylor bubble U_r is about U_{b0}. This suggests that the shape of the nose of the Taylor bubble at point B remains close to that in stagnant fluid. Therefore the curvature ξ_0 at the nose of the Taylor bubble without oscillation: $\xi_B \simeq \xi_0$, and $\xi_0 \simeq 5.3/D$ according to Dumitrescu (1943).

In the following, the effects of the relative velocities will be assumed small comparatively to the effects of the surface tension, gravity and inertia forces. In other words the quasi-hydrostatic situation in the oscillating reference frame is assumed. In these conditions we have:

$$P_i + \rho_i g Z(1 - a\sin\omega t) = cste = C_i \tag{9}$$

where the subscript i stands for liquid (l) or gas (g), and Z is the vertical coordinate of the point defined by starting from the top of the tube (see Fig. 9). Over one period T, Z can be considered constant ($Z < 0$), and thus Eq. (9) is reduced to:

$$P_i - \rho_i g Z a \sin\omega t = cste = C_i' \tag{10}$$

By writing Eq. (10) in the liquid and gas and by taking into account that $P_g - P_l = \sigma\xi$ at the nose of the bubble, we obtain:

$$\sigma(\xi - \xi_0) + (\rho_l - \rho_g) g Z \sin\omega t = 0 \tag{11}$$

where the reference time $t = 0$ is taken at point B.

- At point B, $t = 0$ and $\xi = \xi_0$, the classic situation: $\xi = \xi_0$ and $U_b \simeq U_{b0}$, is found, as described previously.
- At point A: $t = -T/4$, Eq. (11) leads to $\xi_A < \xi_0$. In other words, the nose of the Taylor bubble flattens, as shown in Fig. 9 (position A). Consequently, the flow of the downward liquid Q_w and also the velocity U_r of the bubble decrease (because $U_b \sim Q_w$). This is in agreement with the results of measurement indicated in Fig. 8c.

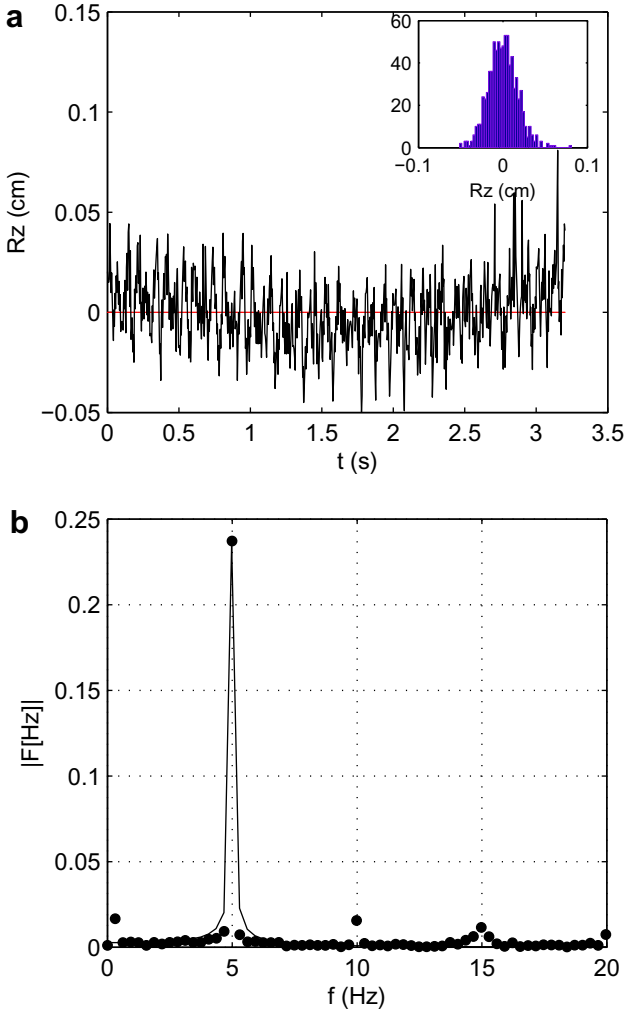

Fig. 7. (a) Residue between the measured and optimized positions of the bubble, (b) spectrum, $f = 5$ Hz and $b = 5$ mm.

– At point C: $t = T/4$, Eq. (11) leads to $\xi_C > \xi_0$. In other words the nose of the Taylor bubble adopts a curvature higher than in the stagnant case, as is shown in Fig. 9 (position C). Consequently, the flow of the downward liquid Q_w and also the velocity U_r of the bubble increase (because $U_b \sim Q_w$). This is in agreement with the results of measurement indicated in the Fig. 8c.

Moreover, at point A, the curvature ξ_A decreases and can even reverse and change the sign when the relative acceleration a increases. The experiment shows that there exists a critical value a_c, from which an interface disturbance is formed. This disturbance is propagated downward the Taylor bubble in the form of a wave, as it is indicated in the Fig. 9 and on the photograph in Fig. 10. Its evolution over time against the bubble nose is shown in Fig. 8e. The mean velocity of convection of the wave relatively to the nose of the bubble is about $l/(T/2)$ where l is the length of the bubble, and the maximum velocity reached remains close to the velocity of the liquid in film. This last point will be clarified in a forthcoming work by making changes to the test section which make it possible to enhance precision in determining the interface deformation and the behavior of the film. We are also interested in a predictive model allowing to evaluate a_c.

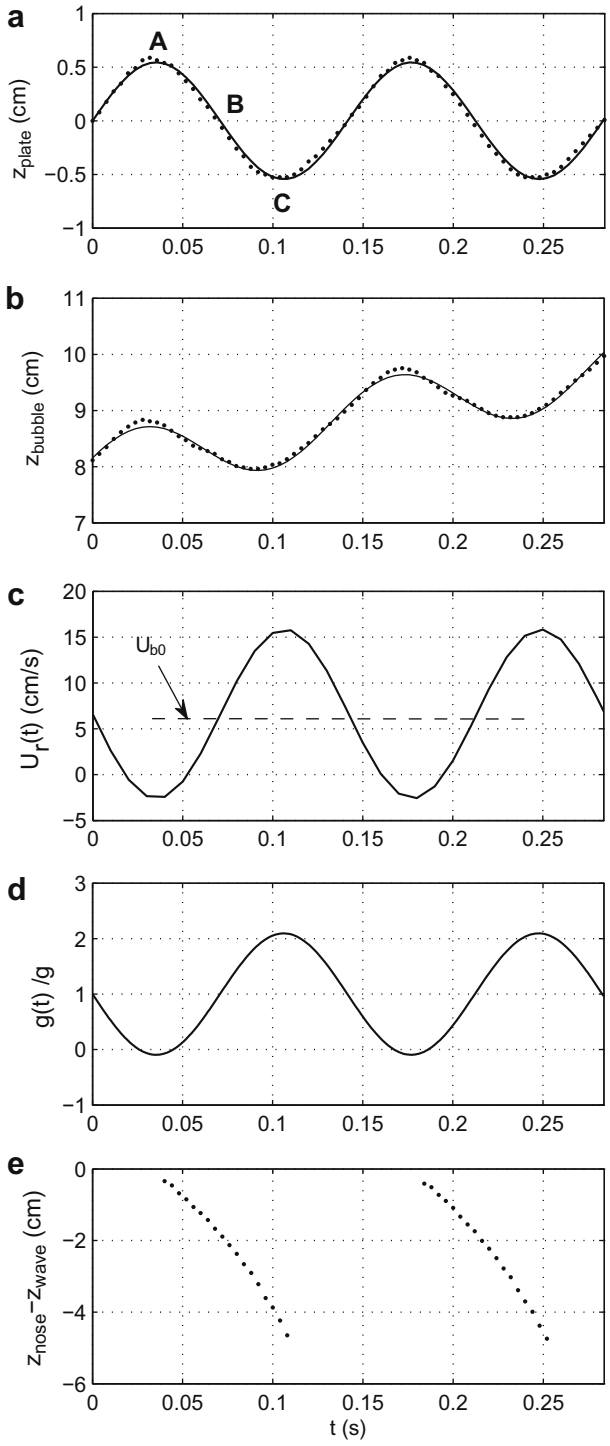

Fig. 8. Temporal evolutions of: (a) plate position, (b) bubble position, (c) relative velocity, (d) effective acceleration $\frac{g(t)}{g} = 1 - a\sin\omega t$, and (e) wave position, for water, $f = 7$ Hz, $b = 5$ mm, $D = 9.8$ mm. In this experiment $U_{b0} \simeq 1.04\bar{U}_b$.

3.2. Pipe diameter effect on the Taylor bubble motion

To examine the pipe diameter effect, the bubble motion in water for two pipes with internal diameters of 9.8 mm and 20 mm is studied for different frequencies.

The mean rise velocity $\bar{U}_b$ evolution with the relative acceleration a is shown in Fig. 11. We can observe that when the pipe is not subjected to the oscillating motion, the mean rise velocity for the two pipe diameters is, respectively, $U_{b0} = 6.9$ cm/s and

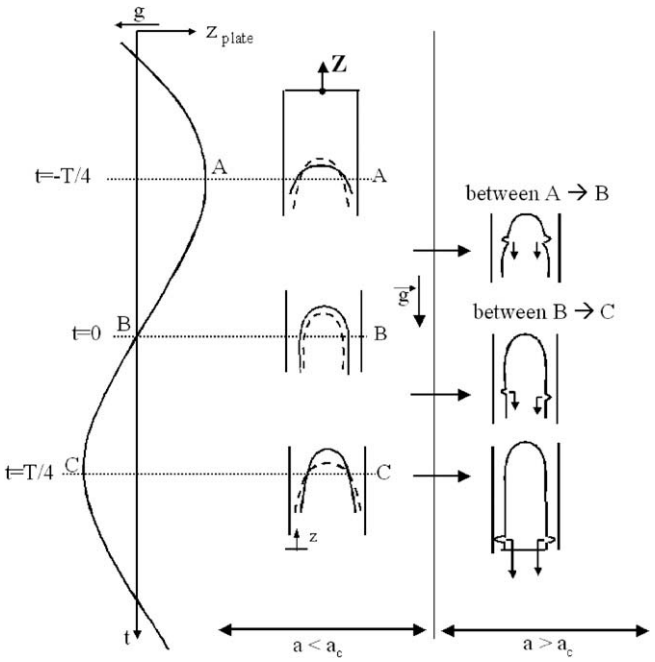

Fig. 9. Sketch of bubble nose deformation during one half period. The dashed line corresponds to the shape of the Taylor bubble in stagnant fluid. The right-hand part of the figure is a sketch of the formation of the wave at the nose and shows its convection downward to the bottom.

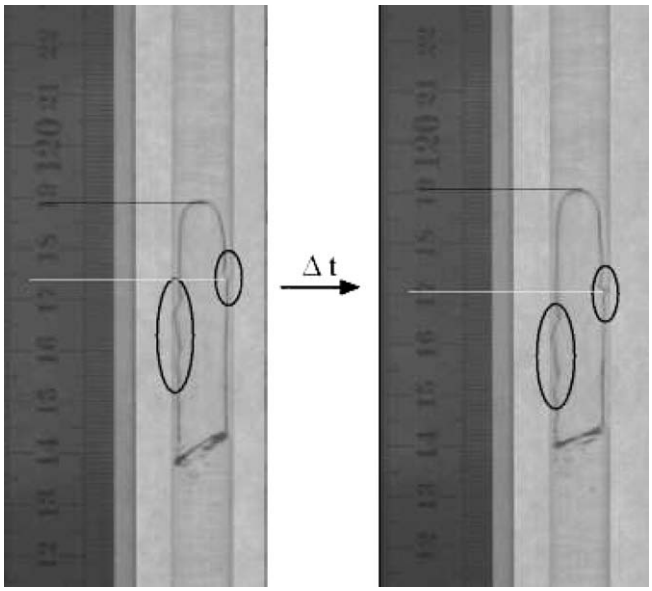

Fig. 10. Photograph of the Taylor bubble at $t = t_0$ and $t = t_0 + \Delta t$, $\Delta t = 0.008$ s, for $f = 7$ Hz, $D = 9.8$ mm, $a = 1.08$ – appearance of wave propagation.

$U_{b0} = 14.5$ cm/s. Given these values and using Eq. (1), the Froude number is, respectively, equal to 0.22 and 0.327 with the corresponding Bond number of 13.05 and 54.4. Thus for the pipe with the smaller diameter the Froude number obtained is almost the same as that obtained using Eq. (2) (~ 0.23) in which the surface tension effects are taken into account. For the pipe with a diameter of 20 mm the Froude number obtained agrees much more to that obtained by Davies and Taylor (1950) (0.328). These results are consistent with those published in the literature for both cases, with or without surface tension effect.

Under relative acceleration, the bubble mean rise velocity $\bar{U}_b$ decreases until a critical value of the acceleration a, where the velocity starts increasing. This tendency is the same for both pipe diameters but it seems that for $D = 20$ mm, the velocity increase occurs when the relative acceleration is greater than $a_c \simeq 1.5$ while for $D = 9.8$ mm the velocity increase can be observed from $a_c \simeq 1$. By analyzing the images obtained by camera and for the two pipe diameters, we can observe when $a > a_c$ the creation of small waves which move downward along the bubble and accelerate slightly the bubble motion by pushing the liquid film downward as shown in Fig. 10. This can probably explain the increase in rise velocity after the critical relative acceleration. Nevertheless, there could be another reason for the bubble velocity increase beyond a_c. As can be seen in Fig. 10 the two waves on both sides of the bubble are not symmetric. This will cause the bubble to be unaxisymmetric similar to the situation described by Kubie (2000) in horizontally oscillating vertical pipes. In this case the downward liquid film flow rate increases in one side, and, as does the velocity of the Taylor bubble as a consequence.

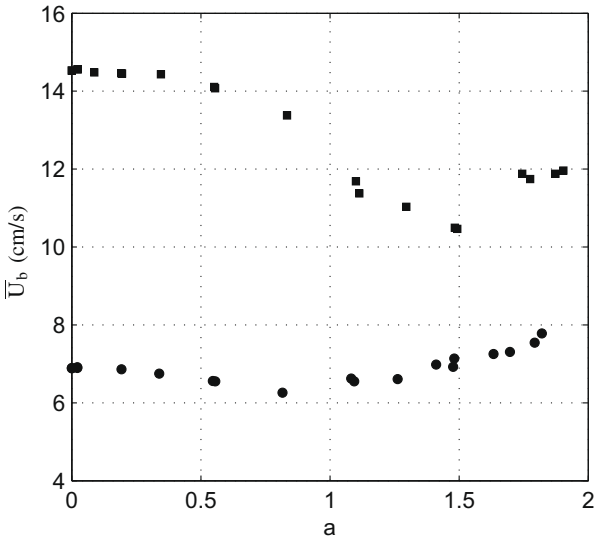

Fig. 11. Evolution of the bubble mean rise velocity, $\bar{U}_b$ with the relative acceleration a, for water: •, $D = 9.8$ mm; ■, $D = 20$ mm.

In order to compare our experimental results with the bubble rise velocity results obtained by Brannock and Kubie (1996), Clanet et al. (2004), the velocity ratio, $\bar{U}_b/U_{b0}$ is plotted versus the relative acceleration, a, in Fig. 12. As shown, for both experimental results of Brannock and Kubie (1996) and analytical results of Clanet et al. (2004), the velocity ratio, $\bar{U}_b/U_{b0}$ decreases as the relative acceleration increases and this for all of the relative acceleration values. As we can see, at the beginning our results concerning the pipe diameter of 20 mm agree well with their results obtained for the pipe diameter of 22 mm. But from $a \simeq 1$ up to $a \simeq 1.5$ the velocity ratio decrease in our case is more significant (the difference is about 10%). From $a \simeq 1.5$ the velocity ratio increases in our experiments without any break of the bubble contrary to the observations of Brannock and Kubie. These authors report that for a relative acceleration greater than 1.6, the bubble is broken. This difference in the ratio $\bar{U}_b/U_{b0}$ may be due to the way of determining the bubble mean rise velocity employed by Brannock and Kubie (1996). They measured the mean velocity by $\bar{U}_b = L/t$ where L is a fix distance of 1500 mm and t is the time taken by the bubbles to cover this distance. This method is correct only when the time t is a multiple of the period T ($t = nT, n \in N$). Consequently, the measurements of $\bar{U}_b$ by Brannock and Kubie (1996) cannot be considered very accurate. For the pipe diameter of 9.8 mm not presented in Fig. 12, because no direct comparison with Brannock or Clanet was available, the tendency observed by Brannock is only

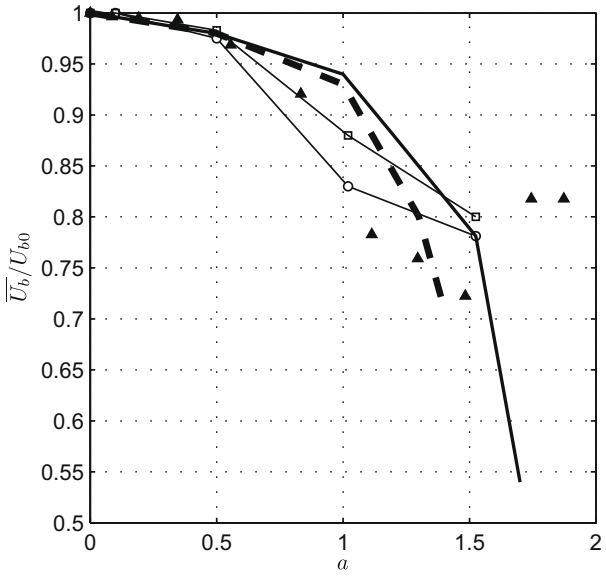

Fig. 12. Ratio $\bar{U}_b/U_{b0}$ vs a, comparison with Brannock and Kubie (1996) and Clanet et al. (2004): present experimental work: ▲, $D = 20$ mm; previous works: —○—, Brannock and Kubie ($D = 22$ mm); —□—, Brannock and Kubie ($D = 44$ mm); — —, Clanet et al. ($D = 22$ mm); ——, Clanet et al., ($D = 44$ mm).

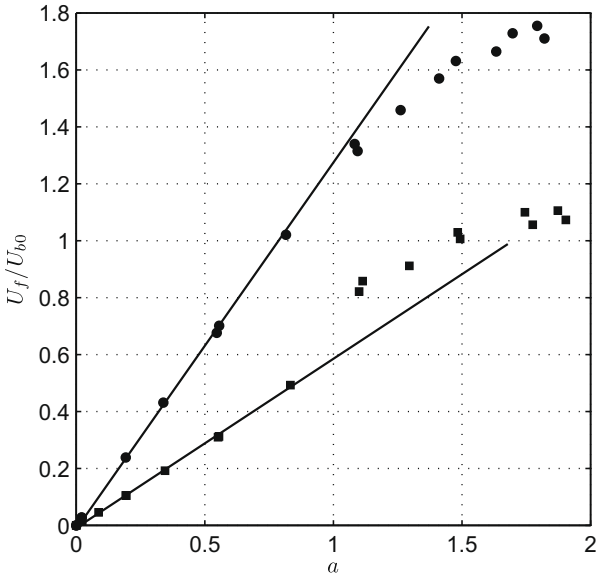

Fig. 13. Ratio U_f/U_{b0} vs relative acceleration, a for water: •, $D = 9.8$ mm; ■, $D = 20$ mm. Solid line: linear best fit.

confirmed for very weak relative accelerations ($a < 1$). As the pipe diameter is smaller than 20 mm, the effect of the surface tension becomes important, which might cause the difference in the results.

The fluctuating velocity U_f evolution with the relative acceleration is first linear and then deviates from the linear trend (Fig. 13). For $D = 9.8$ mm the fluctuating velocity increase follows the linear evolution up to $a = 1$ and then deviates and slows down with increasing the relative acceleration. For $D = 20$ mm there is a first jump from the linear tendency and subsequently a slowdown trend. The line slope of the ratio U_f/U_{b_0} versus a is 1.24 and 0.58, respectively. As illustrated in this figure, the fluctuant velocity decreases as the pipe diameter increases.

3.3. Influence of Liquid physical properties on the Taylor bubble motion

In this section, we present the experimental results obtained for a Taylor bubble moving in a pipe of 9.8 mm diameter. Four low viscous test liquids are tested in order to study the effects of the surface tension. For the case of bubble motion in a stagnant liquid, the experimental results obtained are in good agreement with Fabre and Line (1992) correlation (Eq. (2)) as shown in Fig. 14 and in Table 2.

For the four fluids used, the evolution of the mean velocity ratio, $\bar{U}_b/U_{b0}$, with the relative acceleration is plotted in Fig. 15. As described in the previous section, two zones can be distinguished. The zone in which the velocity ratio decreases as the relative acceleration increases and the zone in which the velocity ratio increases with the relative acceleration. As shown in Fig. 15, this tendency is the same for the four fluids used. For $a < 1$, our results show that the velocity ratio $\bar{U}_b/U_{b0}$ does not depend on the ratio l_c/D and remains in the same order as that found by Brannock and Kubie and Clanet et al. For $a > 1$, it can be noted that except for water in the small pipe, the ratio $l_c/D(= \sqrt{2/Bo})$ does not seem to influence the evolution of the velocity ratio $\bar{U}_b/U_{b0}$. This probably suggests a critical value of $(l_c/D)_c$ in the range of 0.3–0.39 such as for $l_c/D < (l_c/D)_c$, variations of $\bar{U}_b/U_{b0}$ do not depend on this parameter. At this stage, we can not give a physical explanation taking into account the complexity of the problem.

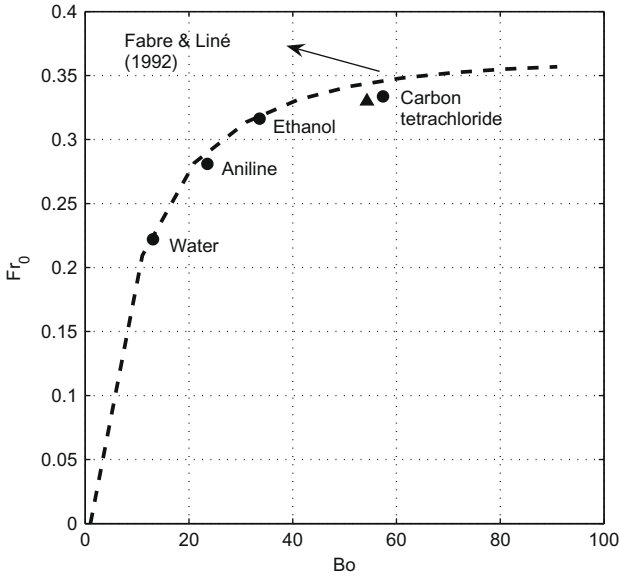

Fig. 14. Evolution of Froude number in four liquids, without oscillation, $D = 9.8$ mm, •; water $D = 20$ mm, ▲.

Table 2
Froude and Bond number values for stagnant fluids without oscillation, comparison with Fabre and Line (1992).

Fluid	D (mm)	Fr_0	Bo	% Difference with Fabre
Water	9.8	0.22	13.05	0.9
Aniline	9.8	0.28	23.55	2.8
Ethanol	9.8	0.32	33.62	0.6
Carbon tetrachloride	9.8	0.33	57.4	3.6
Water	20	0.33	54.3	4

In Fig. 16, the evolution of the fluctuating velocity with the relative acceleration for the four test fluids is shown. We also add on this figure the results concerning the bubble motion in water in the pipe of 20 mm diameter. As illustrated, the evolution is linear for $a < 1$. It can be remarked that for Carbon tetrachloride one data

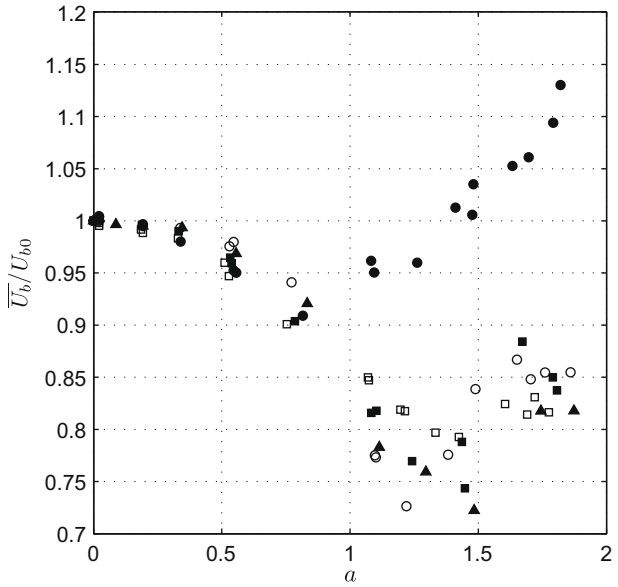

Fig. 15. Ratio $\bar{U}_b/U_{b0}$ versus the relative acceleration, a: •, water; ■, ethanol; ◦, carbon tetrachloride; □, aniline; ▲, water ($D = 20$ mm).

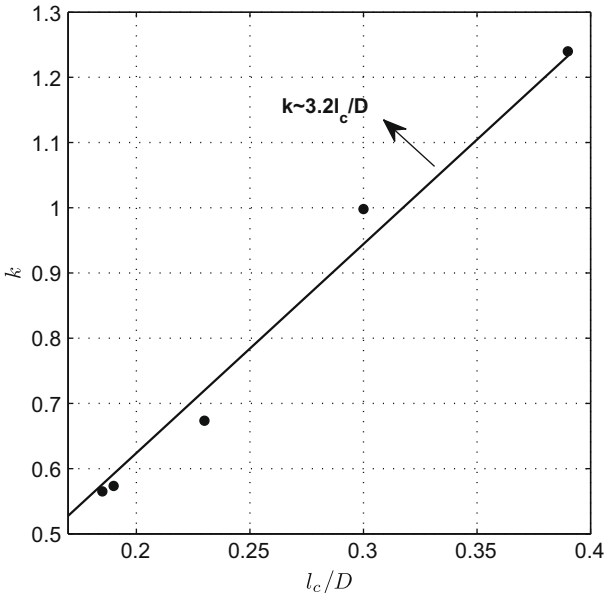

Fig. 17. k versus l_c/D for the four fluids ($D = 9.8$ mm) and for water ($D = 20$ mm).

point ($a = 0.77, U_f/U_{b0} = 0.78$) does not follow the linear behavior but can be considered as outlier. So the general behavior for Carbon tetrachloride is also a linear one for $a < 1$. Beyond this range, the evolution is not linear anymore. It can be seen that decreasing l_c/D decreases the line slope. For bubble motion in ethanol, carbon tetrachloride and in water when the pipe diameter is 20 mm, the results obtained are almost the same. It can be noted that for these three cases the ratio l_c/D remains almost constant ($\simeq 0.2$). Thus from these results we can exhibit the influence of the ratio l_c/D on the fluctuating velocity evolution. For the range $a < a_c$, the ratio $\bar{U}_f/U_{b0}$ can be written as: $U_f/U_{b0} \sim ka$. And by estimating k plotted versus l_c/D (Fig. 17), we obtain: $k \simeq 3.2 l_c/D = 3.2\sqrt{2/Bo}$. So, a correlation of the ratio $\bar{U}_f/U_{b0}$ can be proposed:

$$U_f/U_{b0} \simeq \frac{4.5}{\sqrt{Bo}} a \tag{12}$$

The maximum difference between the data points and the above correlation is about ±7%. From this correlation, it seems that when $Bo \to \infty$, the fluctuating velocity, U_f, tends to zero which means that the bubble does not oscillate at high Bond numbers. Future experiments are required in order to confirm and explain this probable behavior.

3.4. Comparison with Clanet et al. (2004) model

In order to compare our experimental data with the numerical results, Eq. (4) is solved numerically by using the 4th/5th-order Runge–Kutta method. For each testing liquid and for $D = 9.8$ mm and $D = 20$ mm, the instantaneous bubble velocity $U_b(t)$ is thus de-

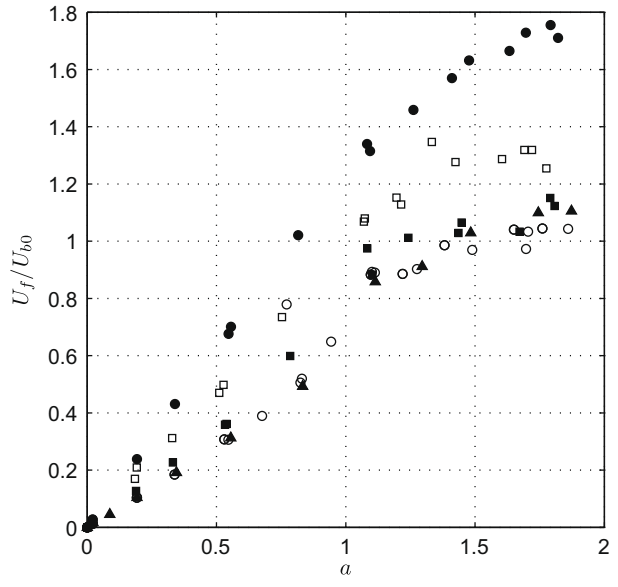

Fig. 16. Ratio U_f/U_{b_0} versus relative acceleration: •, water $l_c/D = 0.39$; ■, ethanol $l_c/D = 0.23$; ◦, carbon tetrachloride $l_c/D = 0.19$; □, aniline $l_c/D = 0.3$; ▲, water ($D = 20$ mm) $l_c/D = 0.19$.

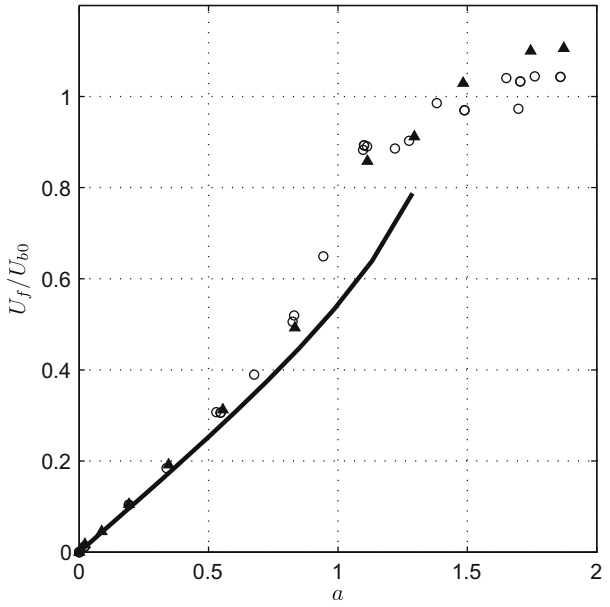

Fig. 18. Ratio U_f/U_{b_0} versus relative acceleration: ◦, carbon tetrachloride; ▲, water ($D = 20$ mm); —, numerical integration of Eq. (4), $D = 9.8$ mm and $Fr_0 = 0.33$.

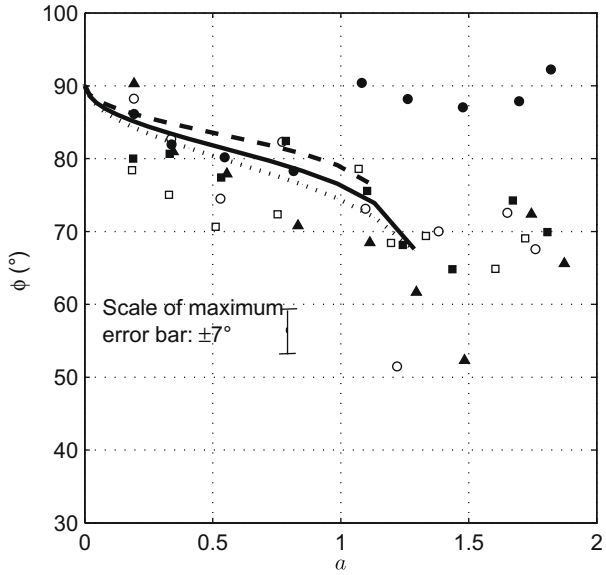

Fig. 19. Phase shifts ϕ between the oscillating plate and the bubble versus relative acceleration, a: experimental work: •, water; ■, ethanol; ○, carbon tetrachloride; □, aniline; ▲, water ($D = 20$ mm); numerical integration: – –, water, $D = 9.8$ mm, $Fr_0 = 0.22$; —, aniline, $D = 9.8$ mm, $Fr_0 = 0.28$; · · ·, ethanol and carbon tetrachloride ($D = 9.8$ mm), water ($D = 20$ mm), $Fr_0 = 0.33$.

duced. By using the relation $k_0 = 1/Fr_0^2 D$, the value of k_0 is adjusted for our cases of study. Then by using the least square fitting method as described in the previous paragraphs, the fluctuating velocity, the mean rise velocity and the phase shift were obtained and compared to our experimental results. It should be noted that in the numerical approach the surface tension effects are considered to be negligible and the bubble nose is assumed to be undeformable. Thus we expect that Eq. (4) provides a good prediction of bubble dynamics when $l_c/D \simeq 0.2$ and for the range of relative acceleration $a < 1$. In these conditions we approach the horizontal asymptote (Fig. 14) where the surface tension effects can be neglected and the bubble can be considered to be undeformable because $a < 1$. As shown in Fig. 18, for $l_c/D \simeq 0.2$ (Carbon tetrachloride and Water for $D = 20$ mm) the numerical solution agrees well with the experimental results for the range of $a < 1$. Beyond this limit the bubble cannot be considered stable and the bubble nose deformation with time should be taken into account. So, it would be interesting to quantify the interface deformation according to the oscillation frequency. This work requires modifications of the test column and will be carried out in the near future.

The phase shifts ϕ between the Taylor bubble and the oscillating plate are plotted in Fig. 19. The maximum error made here is about $\pm 7°$. For very weak relative accelerations the phase shift remains almost constant ($\simeq 90°$) and then decreases slowly. Here, as observed for mean velocity ratios, two zones can be distinguished. The phase shift decrease occurs in the limit $a < 1$. This tendency is well predicted by the numerical results. Beyond this limit it increases with a. As it can be seen, the results dispersion does not allow to predict the exact behavior and future studies are required on this subject.

3.5. Unsteady condition effects

As explained above, by increasing the oscillation frequency the fluctuating velocity increases. Fluctuating velocity becomes greater than the mean rise velocity for high frequencies. In this case and from the Eq. (8), the instantaneous relative velocity becomes negative which means that in each period a downward motion of the bubble can be observed. In Fig. 20, the evolution of the relative velocity in time is compared for two frequencies. While in case (a) (Fig. 20a) there is no downward motion and the relative velocity is positive, when increasing the frequency, negative relative velocity values will appear.

In order to study the effects of quasi-steadiness, we change the definition of the Froude and Bond numbers such as: $\tilde{Fr} = U_r(t)/\sqrt{gD(1 - a\sin\omega t)}$, $\tilde{Bo} = (\rho_L - \rho_G)gD^2[1 - a\sin\omega t]/\sigma$.

For $a = 0$, we recover the classical definition. As for high frequencies ($a > 1$) the term $gD(1 - a\sin\omega t)$ becomes negative, the above expressions are used only for the relative accelerations smaller than one ($a < 1$). Fig. 21 presents the computed results from experimental data, for the frequency of 5 Hz and for the four test liquids where Froude number, $\tilde{Fr}$, is plotted as a function of Bond, $\tilde{Bo}$. On the same graph, the relation $Fr - Bo$ proposed by Fabre and Line (1992) for the case in which the Taylor bubble rises in a quiescent fluid is also plotted. It can be seen that the evolution of Froude with Bond is close to an ellipsoidal form. The "ellipse" center remains the same whatever the oscillation frequency and is located on the steady curve (Fig. 22). By increasing the frequency the ellipse thickens horizontally (Fig. 22). In fact, in this case, the effects of quasi-steadiness become more significant. Consequently,

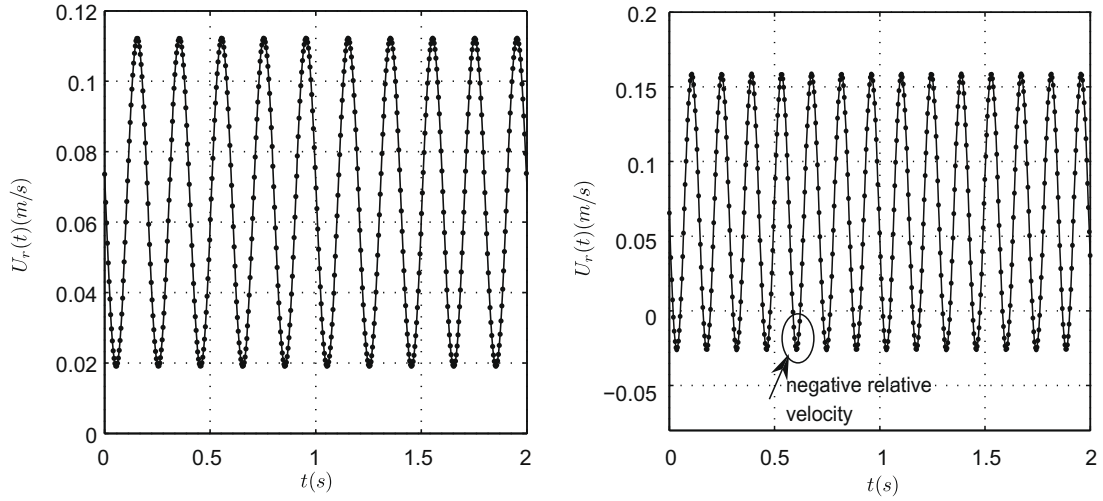

Fig. 20. Relative velocity evolution: (a) water, $f = 5$ Hz; (b) water, $f = 7$ Hz, $D = 9.8$ mm.

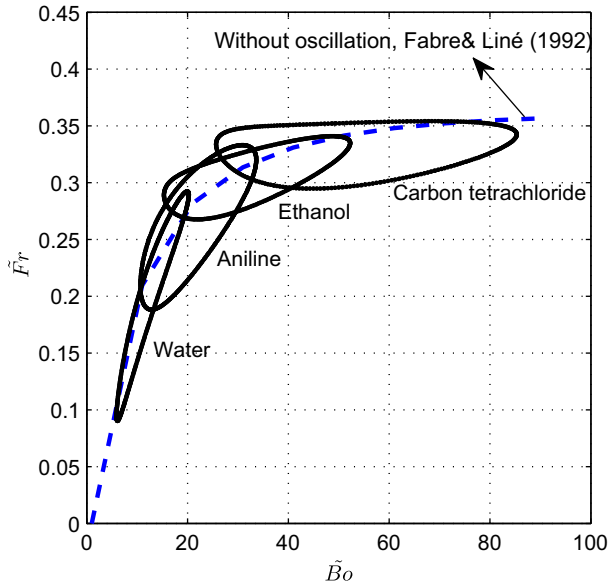

Fig. 21. Froude number evolution in four liquids: $D = 9.8$ mm, $f = 5$ Hz.

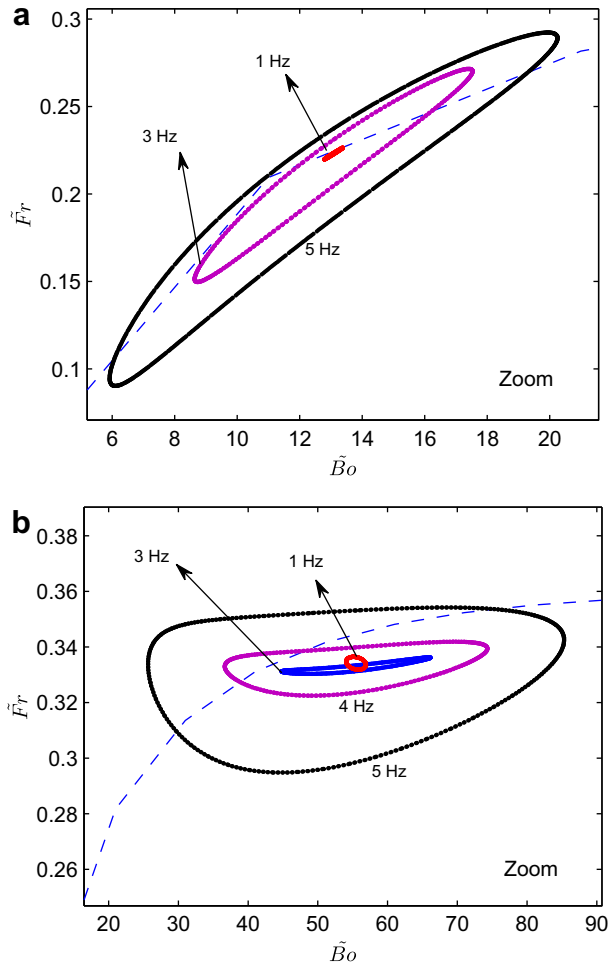

Fig. 22. Froude number evolution for different frequencies: (a) water, (b) carbon tetrachloride, $D = 9.8$ mm.

the Eq. (2) which relates the Froude number to the Bond number cannot be used in unsteady state flows.

4. Conclusion

In this paper we present an experimental study of unsteady Taylor bubble motion in vertical oscillating pipes. The previous works on this subject were limited to the determination of the mean rise velocity of the bubble. In this study, by using video tracking techniques, image processing and numerical processing, accurate measurements of bubble mean and fluctuating velocity and oscillation magnitude were carried out for different frequencies.

The physical mechanism of the bubble propagation was described by an elementary model. The bubble behavior (the deformation of the interface and the formation of the wave) was discussed in three cases corresponding to the three positions of the oscillating plate over a period. Three cases were observed and justified: a classic situation in which the bubble nose shape is such as that in stagnant fluid, the case in which the bubble nose flattens and the case were the radius of curvature of the bubble nose is higher than that while rising in the stagnant fluid.

The influence of the pipe diameter and the liquid physical properties on the unsteady dynamics of long bubbles in vertical tubes was studied. The evolution of the mean rise velocity reveals no clear influence of the ratio l_c/D. The only evident observation is the different behavior of $\bar{U}_b/U_{b0}$ depending whether $a < 1$ or $a > 1$. For $a < 1$, the velocity ratio $\bar{U}_b/U_{b0}$ does not depend on the ratio l_c/D and remains in the same order as that found in previous works. For $a > 1$, it seems that there is a critical value of l_c/D below which variations of $\bar{U}_b/U_{b0}$ do not depend on this parameter. The increase of the mean rise velocity for high relative accelerations seems to be related to the wave formation on both sides of the bubble. The fluctuating velocity, U_f, evolves linearly when $a < 1$ and the line slope decreases by decreasing l_c/D. In this case it was possible to propose a correlation to estimate U_f/U_{b0}.

The numerical results obtained by neglecting surface tension effects, using Clanet's differential equation, could not predict well the velocity evolution in particular for small Froude numbers and pipe diameter. The effects of quasi-steadiness which become more important by increasing the oscillation frequency were also studied by determining Froude and Bond numbers.

In the future, this experimental study may be extended to study the unsteady force acting on the Taylor bubble at intermediate Reynolds numbers. The bubble deformations will be studied in detail in order to determine the interface characteristics and the wave formation in high frequencies. Study of the entire flow field around a Taylor bubble using a PIV technique will be also useful. The works of van Hout et al. (2002), Sousa et al. (2005), Nogueira et al. (2006) will lead us to determine precisely the bubble interface shape as well as the velocity profiles in the liquid film, nose and wake regions.

Acknowledgment

The authors thank Mr. Jean-François Nominé (Translation unit, INIST-CNRS (Institute for Scientific and Technical Information)).

References

Abbad, M., Souhar, M., 2004. Effects of the history force on an oscillating rigid sphere at low Reynolds number. Exp. Fluids 36, 775–782.
Bendiksen, K.H., 1985. An experimental investigation of the motion of long bubbles in inclined tubes. Int. J. Multiphase Flow 11, 797–812.
Brannock, D., Kubie, J., 1996. Velocity of long bubbles in oscillating vertical pipes. Int. J. Multiphase Flow 22, 1031–1034.
Clanet, C., Heraud, P., Searby, G., 2004. On the motion of bubbles in vertical tubes of arbitrary cross-sections: some complements to the Dumitrescu Taylor problem. J. Fluid Mech. 19, 359–376.
Coleman, T.F., Li, Y., 1996. An interior, trust region approach for nonlinear minimization subject to bounds. SIAM J. Optim. 6, 418–445.

Collins, R., DeMoraes, F.F., Harrison, D., 1978. The motion of a large gas bubble rising through liquid flowing in a tube. J. Fluid Mech. 89, 497–514.
Davies, R.M., Taylor, G.I., 1950. The mechanics of large bubbles rising through extended liquids and through liquids in tubes. Proc. R. Soc. Lond. 200, 375–390.
Dumitrescu, D.T., 1943. Stromung einer lufiblase in sechrecten rohr. ZAMM 23, 139–149.
Fabre, J., Line, A., 1992. Modeling of two-phase slug flow. Ann. Rev. Fluid Mech. 24, 21–46.
Kubie, J., 2000. Velocity of long bubbles in horizontally oscillating vertical pipes. Int. J. Multiphase Flow 26, 339–349.
Madani, S., Caballina, O., Souhar, M., 2007. Some experimentation on a Taylor bubble in an oscillating frame. In: Proceedings of the 6th International Conference on Multiphase Flow, Leipzig, Germany.
Nicklin, D.J., Wilkes, J.O., Davidson, J.F., 1962. Two-phase flow in vertical tubes. Tram. Instn. Chem. Engn. 40, 61–68.
Nogueira, S., Riethmuler, M.L., Campos, J.B.M.L., Pinto, A.M.F.R., 2006. Flow patterns in the wake of a Taylor bubble rising through vertical columns of stagnant and flowing newtonian liquids: an experimental study. Chem. Eng. Sci. 61, 7199–7212.
Sousa, R.G., Riethmuller, M.L., Pinto, A.M.F.R., Campos, J.B.L.M., 2005. Flow around individual Taylor bubbles rising in stagnant cmc solutions: PIV measurements. Chem. Eng. Sci. 60, 1859–1873.
Tung, K.W., Parlange, J.Y., 1976. On the motion of long bubbles in closed tubes – influence of surface tension. Acta Mech. 24, 313–317.
van Hout, R., Gulitsky, A., Barnea, D., Shemer, L., 2002. Experimental investigation of the velocity field induced by a Taylor bubble rising in stagnant water. Int. J. Multiphase Flow 29, 579–596.
White, E.T., Beardmore, R.H., 1962. The velocity of rise of single cylindrical air bubbles through liquids contained in vertical tubes. Chem. Eng. Sci. 17, 351–361.
Zukoski, E.E., 1966. Influence of viscosity, surface tension and inclination angle on motion of long bubbles in closed tubes. J. Fluid Mech. 25, 821–837.